Paraxial approximations to the acoustic VTI wave equation

R. Aleixo, D. Amazonas, F. Silva Neto, and J. Schleicher, UNICAMP and UFPA

Abstract

Many migration methods are based on paraxial approximations to the wave equation. These approximations are used to describe the wave propagation in a preferred direction. We apply the idea of a directed propagation to the so-called anisotropic acoustic wave equation. We derive paraxial approximations for this equation, the first ones being generalizations of the 15° and 45° approximations to the isotropic acoustic wave equation. Moreover, we derive higher-order approximations using Padé approximations. A set of numerical experiments demonstrates that our paraxial equations provide reasonable approximations to the solution of the full equation. Moreover, their computational execution is cheaper than using a direct implementation.

Introduction

Seismic imaging uses the information of acoustic or elastic waves propagating in the earth to construct an image of the subsurface structure. For this purpose, a seismic migration is needed that positions the reflection events in time or depth. To apply migration, it is necessary to solve some kind of wave equation.

When using the full elastic or acoustic wave equation, as is the case in reverse time migration, backscattered waves in unwanted directions tend to create artifacts and obfuscate the desired image. For this reason, many migration methods are based on paraxial approximations to the wave equation.

Paraxial wave equation approximations are used to describe wave propagation in a preferred direction (Bamberger et al., 1988a). Paraxial approximations have many applications as to describe ocean acoustics (Jensen et al., 2000), eletromagnetic waves (Bérenger, 1994), and seismic waves. In seismology, paraxial wave-equation approximations have been applied both to scalar and elastic wave propagation (Kern, 1992; Bunks, 1993; Jenner et al., 1997). Numerical computations based on wave approximations are a part of geophysical data processing. The most common approximations are parabolic (or 15°) approximation (Bamberger et al., 1988b) and 45°-approximation (Claerbout, 1976). Since paraxial wave-equation approximations are based on pseudo-differential operators, they tend to have problems at the boundary between transient and evanescent waves. Recent advances using the complex Padé approximation of the involved square root have shown how to minimize these problems (Amazonas et al., 2007).

Up to now, these paraxial approximations have been applied almost exclusively to isotropic wave equations. However, considering anisotropy in seismic imaging is becoming more and more important. Many approximations have been made to describe wave propagation in anisotropic media, for example, using weak elastic anisotropy (Thomsen, 1986) and using ellipical approximations (Helbig, 1983; Dellinger and Muir, 1988). (Alkhalifah, 1998) derived an acoustic approximation for the dispersion relation for P waves in anisotropic media. Using this approximation, Alkhalifah (2000) derived an anisotropic acoustic wave equation for vertical transversely isotropic (VTI) media. While acoustic media can at most exhibit elliptical anisotropy, the equation derived by Alkhalifah (2000) is a good approximation for P waves in VTI media.

In this paper, we combine the idea of a directed propagation with the anisotropic acoustic wave equation of Alkhalifah (2000). We derive two paraxial approximations for this equation. The first set of approximations are generalizations of the 15° and 45° approximations to the isotropic acoustic wave equation. Moreover, we propose higher-order paraxial approximations using the theory of Padé approximations.

The anisotropic acoustic wave equation

By setting the vertical shear wave velocity to zero, Alkhalifah (1998) derived a simple equation that relates the vertical slowness, p_z, to the horizontal one, $p_r = \sqrt{p_x^2 + p_y^2}$, in VTI media. This acoustic approximation to the dispersion relation in VTI media yields accurate kinematic approximations to the actual elastic model (Alkhalifah, 1996, 1998).

The migration dispersion relation in 3-D VTI media is

$$p_z^2 = \frac{v^2}{v_v^2}\left(\frac{1}{v^2} - \frac{p_x^2 + p_y^2}{1 - 2v^2\eta(p_x^2 + p_y^2)}\right), \qquad (1)$$

where v and v_v are the NMO and vertical velocities, respectively, and η is the anellipticity parameter, all assumed to be constant. In terms of the components of the wavenumber vector $\mathbf{k} = \omega\mathbf{p}$, equation (1) can be written as

$$k_z^2 = \frac{v^2}{v_v^2}\left(\frac{\omega^2}{v^2} - \frac{\omega^2\,(k_x^2 + k_y^2)}{\omega^2 - 2v^2\eta(k_x^2 + k_y^2)}\right). \qquad (2)$$

Interpreting k_x, k_y, k_z, and ω as Fourier-domain symbols of the respective partial derivatives, Alkhalifah (2000) derived the anisotropic acoustic wave equation,

$$\frac{\partial^4 u}{\partial t^4} - (1+2\eta)v^2\left(\frac{\partial^4 u}{\partial x^2\partial t^2} + \frac{\partial^4 u}{\partial y^2\partial t^2}\right) = v_v^2\frac{\partial^4 u}{\partial z^2\partial t^2} - 2\eta v^2 v_v^2\left(\frac{\partial^4 u}{\partial x^2\partial z^2} + \frac{\partial^4 u}{\partial y^2\partial z^2}\right). \qquad (3)$$

Note that for isotropic media, where $v_v = v$ and $\eta = 0$, equation (3) reduces to the second time derivative of the isotropic acoustic wave equation.

One-way wave propagation

To describe downgoing waves, we have to take the square root of equation (2) according to

$$k_z = \frac{\omega}{v_v}\left(1 - \frac{v^2\,k_r^2}{\omega^2 - 2v^2\eta k_r^2}\right)^{1/2}, \qquad (4)$$

where $k_r^2 = k_x^2 + k_y^2$. In analogy to the isotropic case (Bamberger et al., 1988a), the symbol of the associated differential equation can thus be represented as

$$\mathcal{L} = v_v\,k_z - \omega\left(1 - X^2\right)^{1/2} = 0\,, \qquad (5)$$

where we have introduced the notation

$$X^2 = \frac{v^2\,k_r^2}{\omega^2 - 2v^2\eta k_r^2}\,. \qquad (6)$$

We observe from equation (5) that the symbol has the same structure as in the isotropic case.

Paraxial approximations

Based on the symbol (5), we can derive paraxial approximations for the anisotropic acoustic wave equation (3). For this purpose, we follow the methodology for the isotropic case (Bamberger et al., 1988a,b).

Parabolic or 15° approximation

For small values of X we can use the first-order Taylor series to approximate $(1 - X^2)^{1/2}$ as

$$\left(1 - X^2\right)^{1/2} = 1 - \frac{1}{2}X^2 + \mathcal{O}(X^4)\,. \qquad (7)$$

In this approximation, the symbol is

$$\mathcal{L} = v_v\,k_z - \omega\left(1 - \frac{1}{2}\,\frac{v^2\,k_r^2}{\omega^2 - 2v^2\eta k_r^2}\right) = 0\,. \qquad (8)$$

Multiplying the above equation by ω and distributing terms, we find

$$v_v\,k_z\omega^3 - 2v_v v^2\eta k_z\omega k_r^2 - \omega^4 + 2v^2\eta\omega^2 k_r^2 + \frac{1}{2}\,\omega^2 v^2\,k_r^2 = 0\,, \qquad (9)$$

which represents the differential equation

$$\frac{\partial^4 u}{\partial t^4} - \left(2v^2\eta + \frac{1}{2}v^2\right)\frac{\partial^4 u}{\partial r^2\partial t^2} + v_v\frac{\partial^4 u}{\partial z\partial t^3} + 2v_v v^2\eta\frac{\partial^4 u}{\partial z\partial t\partial r^2} = 0\,. \qquad (10)$$

Here, $\partial^2/\partial r^2 = \partial^2/\partial x^2 + \partial^2/\partial y^2$. This equation is a generalization of the parabolic (or 15°) isotropic wave equation, to which it reduces when $v_v = v$ and $\eta = 0$.

45° approximation

Equation (10) is a good approximation for small X, i.e., propagation close to the vertical direction. To derive a more accurate equation that describes wave propagation for larger propagation angles, we use a first Padé approximation.

$$\left(1 - X^2\right)^{1/2} = \frac{1 - \frac{3}{4}X^2}{1 - \frac{1}{4}X^2} + \mathcal{O}(X^6), \qquad (11)$$

In this approximation, the symbol is

$$\mathcal{L} = v_v\,k_z - \omega\left(\frac{1 - \frac{3}{4}\frac{v^2\,k_r^2}{\omega^2 - 2v^2\eta k_r^2}}{1 - \frac{1}{4}\frac{v^2\,k_r^2}{\omega^2 - 2v^2\eta k_r^2}}\right) = 0\,. \qquad (12)$$

After distribution of terms, this leads to

$$v_v\,k_z\omega^2 - 2v^2 v_v\eta k_z k_r^2 - \frac{1}{4}v^2\,k_r^2 v_v\,k_z - \omega^3 + 2v^2\eta k_r^2\omega + \frac{3}{4}v^2\,k_r^2\omega = 0\,, \qquad (13)$$

which represents the differential equation

$$\frac{\partial^3 u}{\partial t^3} - \left(2v^2\,\eta\,v_v + \frac{1}{4}v_v v^2\right)\frac{\partial^3 u}{\partial z\partial r^2} + v_v\frac{\partial^3 u}{\partial z\partial t^2} - \left(2v^2\eta + \frac{3}{4}v^2\right)\frac{\partial^3 u}{\partial t\partial r^2} = 0. \qquad (14)$$

This equation is a generalization of the 45° isotropic wave equation, to which it reduces when $v_v = v$ and $\eta = 0$.

Higher-order paraxial approximations

Equations (10) and (14) are based on small-order approximations, describing wave propagation correctly only in a certain range around the vertical axis. If we want to describe near horizontal propagation correctly, we need higher-order approximations. However, using real approximations we run into problems

with evanescent waves, which can be avoided using complex Padé approximations.

For isotropic media, Bamberger et al. (1988a) proposed the use of higher-order complex Padé approximations to expand the symbol in a more accurate form. Note that, the anisotropic symbol [equation (5)] has the same form as the isotropic one (see Bamberger et al., 1988a). Therefore, the anisotropic higher-order approximation has the same structure.

The real Padé approximation of equation (5) has the form (Bamberger et al., 1988a)

$$\mathcal{L} = v_v\, k_z - \omega f_n\left(X^2\right), \tag{15}$$

where

$$f_n\left(X^2\right) = 1 - \sum_{k=1}^{n} \frac{\beta_k X^2}{1-\gamma_k X^2}, \tag{16}$$

is the Padé approximation of the square-root in equation (5). The Padé coefficents are given by

$$\begin{cases} \beta_k = \dfrac{2}{2n+1}\sin^2\left(\dfrac{k\pi}{2n+1}\right), \\ \gamma_k = \cos^2\left(\dfrac{k\pi}{2n+1}\right). \end{cases} \tag{17}$$

After multiplication with the Fourier transform of the wavefield, $\hat{u}$, equation (15) becomes

$$v_v\, k_z \hat{u} - \omega\hat{u} + \omega \sum_{k=1}^{n} \frac{\beta_k X^2}{1-\gamma_k X^2}\hat{u} = 0. \tag{18}$$

Defining, for $1 \le k \le n$,

$$\hat{y}_k = \frac{\beta_k X^2}{1-\gamma_k X^2}\hat{u}, \quad 1 \le k \le n, \tag{19}$$

we can recast equation (18) into the form

$$v_v\, k_z \hat{u} - \omega\hat{u} + \omega \sum_{k=1}^{n} \hat{y}_k = 0. \tag{20}$$

Calculating the inverse Fourier transform of equations (19) and (20), we have

$$\begin{cases} \dfrac{\partial u}{\partial t} + v_v \dfrac{\partial u}{\partial z} - \displaystyle\sum_{k=1}^{n} \frac{\partial y_k}{\partial t} = 0, \\ \dfrac{\partial^2 y_k}{\partial t^2} - (2\eta+\gamma_k)v^2 \dfrac{\partial y_k}{\partial x^2} = \beta_k v^2 \dfrac{\partial^2 u}{\partial x^2}, \end{cases} \tag{21}$$

where v_v and v are the vertical and NMO velocities in the anisotropic medim, respectively. In the isotropic case, with $v_v = v$ and $\eta = 0$, system (21) reduces to

$$\begin{cases} \dfrac{\partial u}{\partial t} + v \dfrac{\partial u}{\partial z} - \displaystyle\sum_{k=1}^{n} \frac{\partial y_k}{\partial t} = 0 \\ \dfrac{\partial^2 y_k}{\partial t^2} - \gamma_k v^2 \dfrac{\partial y_k}{\partial x^2} = \beta_k v^2 \dfrac{\partial^2 u}{\partial x^2}. \end{cases} \tag{22}$$

Thus, for aproximations with n terms in the Padé series, as much in isotropic case as in anisotropic case, we have to solve $n+1$ equations, these being one transport equation in the z direction and n equations in the x direction (Bamberger et al., 1988a).

The real Padé approximation (17) has a problem when the argument of the square-root is negative, i.e., when $X^2 > 1$. In other words, this approximation cannot handle evanescent modes correctly. To overcome this limitations, Millinazzo et al. (1997) propose a complex representation of the Padé approximation using a rotation of the branch cut. The complex Padé approximation is

$$\sqrt{1-X^2} \approx C_0 + \sum_{k=1}^{n} \frac{\mathcal{B}_k X^2}{1+\Gamma_k X^2}, \tag{23}$$

with coefficients

$$\begin{cases} C_0 = e^{i\alpha/2}\left[1 - \displaystyle\sum_{k=1}^{n} \frac{\beta_k(e^{-i\alpha}+1)}{[1-\gamma_k(e^{-i\alpha}+1)]}\right], \\ \mathcal{B}_k = \dfrac{\beta_k e^{-i\alpha/2}}{[1-\gamma_k(e^{-i\alpha}+1)]^2}, \\ \Gamma_k = \dfrac{\gamma_k e^{-i\alpha}}{1-\gamma_k(e^{-i\alpha}+1)}, \end{cases} \tag{24}$$

where β_k and γ_k are defined in equations (17). The values $\mathcal{B}_k$ and Γ_k are the complex Padé coefficients, and α is the rotation angle of the branch cut of the square root in the complex plane.

Using approximation (23), equation (15) takes the form

$$\mathcal{L} = v_v\, k_z - \omega\left(C_0 - \sum_{k=1}^{n} \frac{\mathcal{B}_k X^2}{1-\Gamma_k X^2}\right). \tag{25}$$

Note that when $\alpha = 0$, this expression is identical to equation (15). In analogy to equation (19), we introduce a new $\hat{y}_k$ where the complex Padé coefficients $\mathcal{B}_k$ and Γ_k replace the real ones β_k and γ_k. This leads to the anisotropic system

$$\begin{cases} C_0 \dfrac{\partial u}{\partial t} + v_v \dfrac{\partial u}{\partial z} - \displaystyle\sum_{k=1}^{n} \frac{\partial y_k}{\partial t} = 0 \\ \dfrac{\partial^2 y_k}{\partial t^2} - (2\eta+\Gamma_k)v^2 \dfrac{\partial y_k}{\partial x^2} = \mathcal{B}_k v^2 \dfrac{\partial^2 u}{\partial x^2}, \end{cases} \tag{26}$$

which reduces in the isotropic case to

$$\begin{cases} C_0 \dfrac{\partial u}{\partial t} + v \dfrac{\partial u}{\partial z} - \displaystyle\sum_{k=1}^{n} \frac{\partial y_k}{\partial t} = 0 \\ \dfrac{\partial^2 y_k}{\partial t^2} - \Gamma_k v^2 \dfrac{\partial y_k}{\partial x^2} = \mathcal{B}_k v^2 \dfrac{\partial^2 u}{\partial x^2}. \end{cases} \tag{27}$$

Like in the real case, we have to solve one transport equation in the z direction and n equations in

x direction. Note that systems (26) and (27) have the same structure as systems (21) and (22). Therefore, the computational effort to solve these systems is equivalent. It is to be stressed that systems (26) and (27) are more accurate, because they provide an improved handling of the evanescent modes.

Implementation

For the numerical solution of the anisotropic acoustic wave equation, we consider the pressure field defined by

$$P = \frac{\partial^2 u}{\partial t^2}. \tag{28}$$

Using this definition in equation (3) we have

$$\frac{\partial^2 P}{\partial t^2} = (1+2\eta)v^2\frac{\partial^2 P}{\partial r^2} + v_v^2\frac{\partial^2 P}{\partial z^2} - 2\eta v^2 v_v^2\frac{\partial^4 u}{\partial r^2 \partial z^2}. \tag{29}$$

Equations (28) and (29) represent a system that can be solved in 2D using the following algorithm (Alkhalifah, 2000)

$$\begin{aligned} u^{i+1} &= 2u^i - u^{i-1} + \Delta t^2 P^i \\ P^{i+1} &= 2P^i - P^{i-1} + \Delta t^2 \left(\frac{\partial^2 P}{\partial t^2}\right)^i \end{aligned} \tag{30}$$

at each point (r, z).

To solve the complex Padé paraxial approximations for the anisotropic acoustic wave-equation, we choose a set of indices m, n and l in order to establish a finite-difference scheme with uniform grid spacings Δr, Δz and Δt, i.e., $r_m = r_{min} + m\Delta r$, $z_j = z_{min} + j\Delta z$ and $t_l = t_{min} + l\Delta t$. Consequently, for a fixed k, we denote $u(x_m, k, z_j, t_l) = u^l_{m,j}$. In our examples, $x_{min}, z_{min}, t_{min}$ are zero. A possible finite-difference scheme for system (26) can then be represented as (Strikwerda, 1989)

$$\begin{aligned} u^{l+1}_{m,j} &= u^l_{m,j} + \sum_{k=1}^{n}(y^{l+1,k}_{m,j} - y^{l,k}_{m,j}) - \sigma(u^l_{m,j+1} - u^l_{m,j}) \\ y^{l+1,k}_{m,j} &= 2y^{l,k}_{m,j} - y^{l-1,k}_{m,j} + \alpha_k(y^{l,k}_{m+1,j} - 2y^{l,k}_{m,j} + y^{l,k}_{m-1,j}) \\ &\quad + \delta_k(u^l_{m+1,j} - 2u^l_{m,j} + u^l_{m-1,j}), \end{aligned} \tag{31}$$

where

$$\begin{cases} \sigma &= \dfrac{v_v \Delta t}{C_0 \Delta z}, \\ \alpha_k &= \dfrac{(2\eta + \Gamma_k)v^2\Delta t^2}{\Delta x^2}, \\ \delta_k &= \dfrac{\mathcal{B}_k v^2 \Delta t^2}{\Delta x^2}. \end{cases} \tag{32}$$

Numerical examples

In this section, we show some numerical examples of our paraxial approximations and compare them to the results of the solution of system (30) for the full acoustic anisotropic wave equation. In all examples below, the solution of system (30) required a much smaller Δt than that of system (31), leading to about 10 times higher computation time.

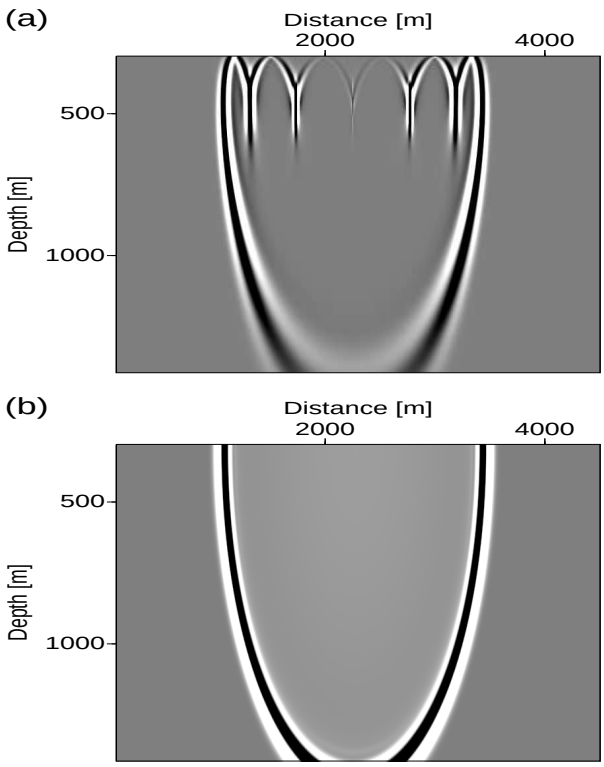

Figure 1: Wavefield at $t = 0.40\ s$ calculated using a homogeneous velocity model with $v = 3500\ km/s$. (a) Paraxial approximation; (b) full equation.

We started by solving the isotropic equation system (27), i.e., $\eta = 0$ and $v_v = v$ in system (31). Figure 1 compares a snapshot of the wavefield in a homogeneous model with $v = 3500$ m/s to the corresponding solution of the full equation, system (30). The source was positioned at 300 m depth. We recognize some artifacts in the top part of the wavefield, which was already reported by Bamberger et al. (1988a). Also, we observe that the shape of the wavefront is slightly distorted and that the paraxial approximation is slightly more dispersive than the full equation.

In our second isotropic test, we used the a smoothed version of the Marmousi velocity model. Figure 2 compares the results for a snapshot at $t = 0.4\ s$. The solution of the full equation in Figure 2b contains upgoing waves which are not present, of course, in Figure 2a. The observations about artifacts in the upper part, wavefront shape and dispersion remain the same as in the homogeneous example.

Next, we tested the anisotropic solution. At first, we solved equation (31) for a homogeneous VTI medium with anisotropy parameters $\epsilon = 0.21$, $\delta = 0.05$, i.e., $\eta \approx 0.15$, and $v_v = 3500\ km/s$. Figure 3 shows the

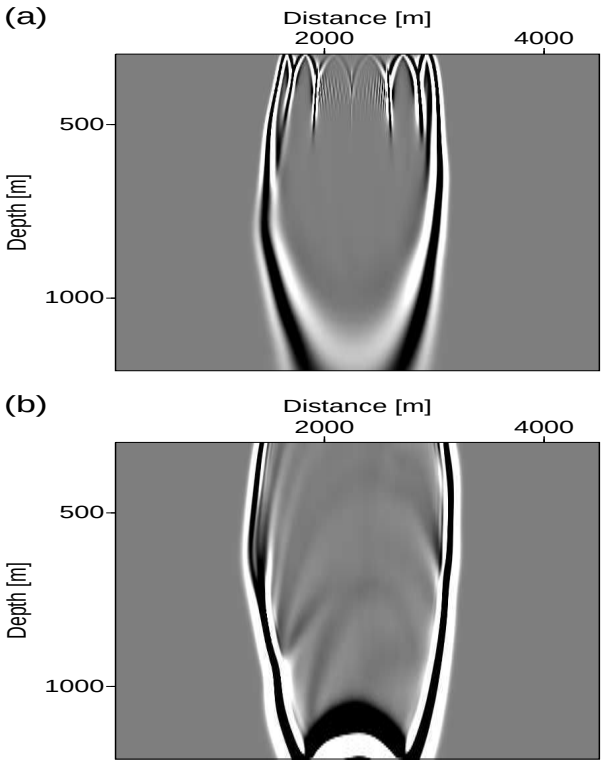

Figure 2: Wavefield in $t = 0.40\ s$ calculated using the Marmousoft velocity model. (a) Paraxial approximation; (b) full equation.

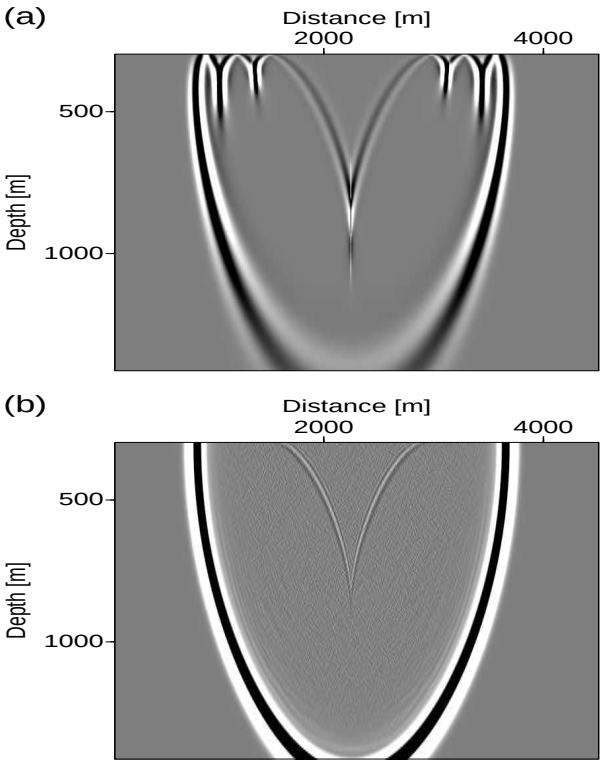

Figure 3: Wavefield in $t = 0.40\ s$ calculated using $\epsilon = 0.21$, $\delta = 0.05$ and $v_v = 3500\ km/s$. (a) Paraxial approximation; (b) full equation.

results for a snapshot at $t = 0.4\ s$. In addition to the observations about wavefront shape, dispersions, and artifacts from the isotropic case, we also see an enhanced pseudo-S wave artifact (Alkhalifah, 2000), but reduced numerical noise when compared to the solution of the full equation.

To reduce the pseudo-S wave artifact, we followed the recipe of Alkhalifah (2000) to place the source in an isotropic region. For this purpose, we repeated the last experiment with a homogeneous, isotropic layer between 240 m and 330 m depth. Figure 4 shows the resulting snapshots. While the pseudo-S wave artifact has been reduced in amplitude, it is still visible in the paraxial approximation (Figure 4a).

Our last numerical example compares the results for a model with three horizontal VTI layers with parameters $\epsilon_1 = 0.21$, $\delta_1 = 0.16$, $v_{v1} = 2200$ m/s, $\epsilon_2 = 0.12$, $\delta_2 = 0.12$, $v_{v2} = 2800$ m/s, $\epsilon_3 = 0.02$, $\delta_3 = 0.02$, $v_{v3} = 3500$ m/s. The source was positioned at 180 m depth. The main features of the snapshots in Figure 5 are the same as observed in the previous examples.

Conclusions

Paraxial approximations to the wave equation are often used when waves propagate in directions close to a preferred direction. In particular, such approximations are used to develop migration methods like those of Collino et al. (1995) and Jenner et al. (1997).

In this paper, we have derived paraxial approximations for the anisotropic acoustic wave equation of Alkhalifah (2000). We have presented equivalents to the 15° and $45°$ wave equations and a higher-order paraxial approximation using Padé approximation.

Our higher-order approximations lead to an equation system system that is equivalent to third-order partial differential equations. Therefore, its computational execution is cheaper than using a direct implementation of Alkhalifah's (2000) equation. We have demonstrated with a set of numerical experiments that our paraxial equations provide reasonable approximations to the solution of Alkhalifah's equation.

Acknowledgments

This work was kindly supported by the Brazilian research agencies CNPq and FAPESP (proc. 06/04410-5), as well as Petrobras and the sponsors of the *Wave Inversion Technology (WIT) Consortium*.

References

Alkhalifah, T., 1996, Analytic insights into the anisotropy parameter η: Center for Wave Phenomena, Colorado School of Mines(CWP-202), 1–22.

———, 1998, Acoustic approximations for processing in transversely isotropic media: Geophysics, **63**, 623–631.

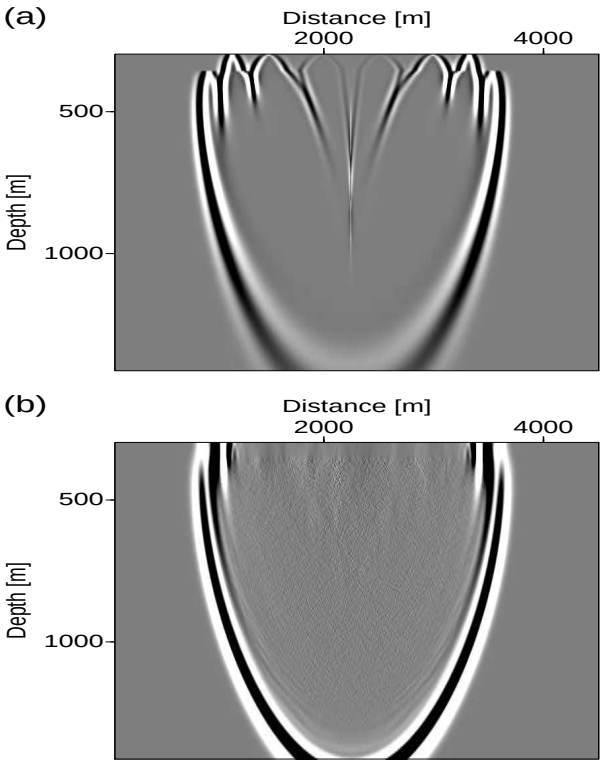

Figure 4: Wavefield in $t = 0.40\ s$ calculated using $\epsilon = 0.21$, $\delta = 0.05$ and $v_v = 3500\ km/s$ with the source in an isotropic medium. (a) Paraxial approximation; (b) full equation.

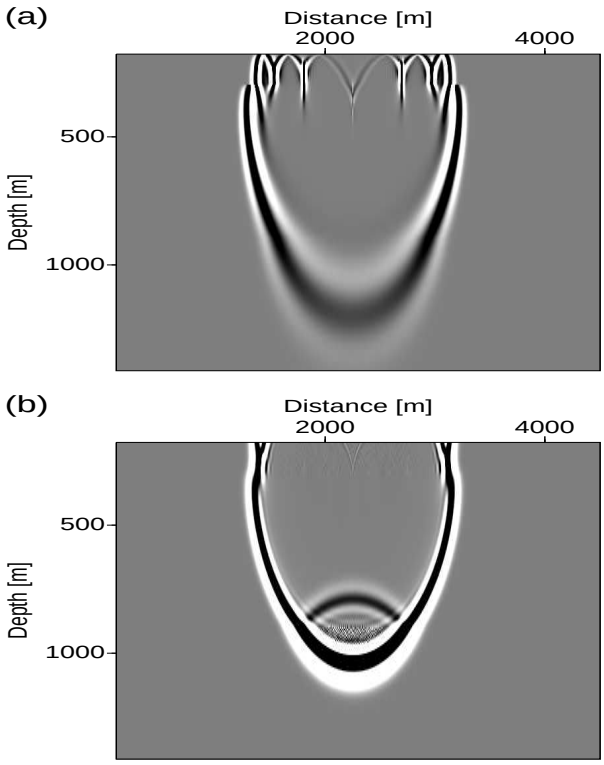

Figure 5: Wavefield in $t = 0.40\ s$ calculated in a heterogeneous anisotropic medium. (a) Paraxial approximation; (b) full equation.

———, 2000, An acoustic wave equation for anisotropic media: Geophysics, **65**, 1239–1250.

Amazonas, D., J. Costa, J. Schleicher, and R. Pestana, 2007, Wide angle FD and FFD migration using complex Padé approximations: Geophysics, **72**, S215–S220.

Bamberger, A., B. Engquist, L. Halpern, and P. Joly, 1988a, Higher order paraxial wave equation approximations in heterogeneuos media: SIAM Journal on Applied Mathematics, **48**, 129–154.

———, 1988b, Parabolic wave equation approximations in heterogeneous media: SIAM Journal on Applied Mathematics, **48**, 99–128.

Bécache, E., F. Collino, and P. Joly, 2000, Higher-order variational finite difference schemes for solving 3-D paraxial wave equations using splitting techniques: Wave Motion, **31**, 101–116.

Bérenger, J.-P., 1994, A perfectly matched layer for the absorption of electromagnetic waves: J. Comput. Phys., **114**, 185–200.

Bunks, C., 1993, Effective filtering of artifacts for finite-difference implementations of paraxial wave equation migration: SEG Technical Program Expanded Abstracts, **12**, 1044–1047.

Claerbout, J., 1976, Fundamentals of geophysical data processing: McGraw-Hill.

Collino, F., M. Kern, and P. Joly, 1995, On two migration methods based on paraxial equations in a 3D heterogeneous medium: Presented at the Mathematical Methods in Geophysical Imaging III. SPIE.

Dellinger, J. and F. Muir, 1988, Imaging reflections in elliptically anisotropic media: Geophysics, **53**, 1616–1618.

Helbig, K., 1983, Elliptical anisotropy—its significance and meaning: Geophysics, **48**, 825–832.

Jenner, E., M. de Hoop, K. Larner, and M. van Stralen, 1997, Imaging using optimal rational approximation to the paraxial wave equation: SEG Technical Program Expanded Abstracts, **16**, 1750–1753.

Jensen, F. B., W. A. Kuperman, M. B. Porter, and H. Schmidt, 2000, Computational ocean acoustics: Springer Verlag.

Kern, M., 1992, Numerical methods for paraxial wave equations in 3-D heterogeneous media: SEG Technical Program Expanded Abstracts, **11**, 909–912.

Millinazzo, F. A., C. A. Zala, and G. H. Brooke, 1997, Square-root approximations for parabolic equation algorithms: J. Acoust. Soc. Am., **101**, 760–766.

Strikwerda, J., 1989, Finite difference schemes and partial differential equations: Wadsworth and Brooks, Inc.

Thomsen, L., 1986, Weak elastic anisotropy: Geophysics, **51**, 1954–1966.